Impact of COVID-19 lockdown on particulate matter oxidative potential at urban background versus traffic sites

Supplementary information

S1. Overview of measurements

Table S1: Overview of measurements available for the GRE and BERN sites.

Study area	Site type	PM size fraction	Variable	Number of observations	Sampling period
Grenoble	Urban background	PM_{10}	PM_{10}	2001	23/01/2008 to 24/04/2022
			OC	2011	23/01/2008 to 24/04/2022
			EC	2010	23/01/2008 to 24/04/2022
			BC_{tot}	1051	02/12/2014 to 30/03/2021
			BC_{wb}	1051	02/12/2014 to 30/03/2021
			BC_{ff}	1051	02/12/2014 to 30/03/2021
			OP_{AA}	1249	02/01/2013 to 24/01/2022
			OP_{DTT}	1249	02/01/2013 to 24/01/2022
Bern	Traffic	PM_{10}	PM_{10}	6837	01/01/2000 to 31/12/2021
			OP_{AA}	273	07/06/2018 to 31/12/2020
			OP_{DTT}	273	07/06/2018 to 31/12/2020
Bern	Traffic	$PM_{2.5}$	$PM_{2.5}$	6885	01/01/2000 to 31/12/2021
			BC_{tot}	2515	01/01/2015 to 31/12/2021
			BC_{wb}	2441	01/01/2015 to 31/12/2021
			BC_{ff}	2441	01/01/2015 to 31/12/2021
			OP_{AA}	177	07/06/2018 to 29/12/2020
			OP_{DTT}	177	07/06/2018 to 29/12/2020

S2. Feature importance scores for the Random Forest (RF) model
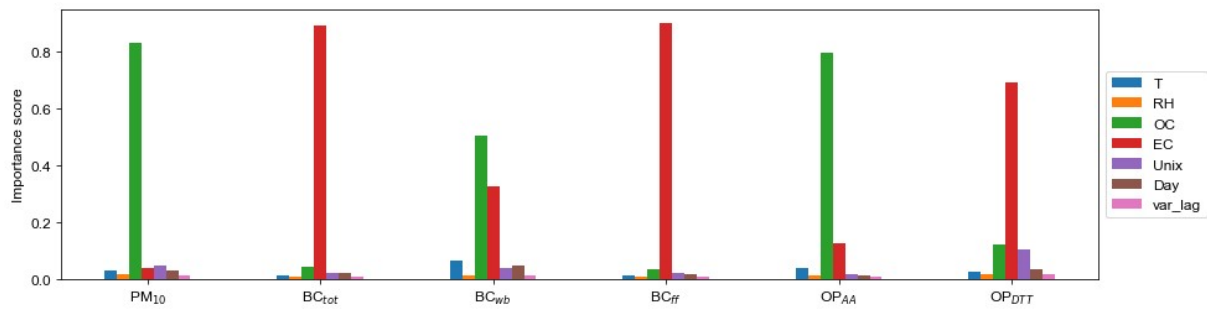

Figure S1: Feature importance score for the RF models performed on each target variable in the GRE site.
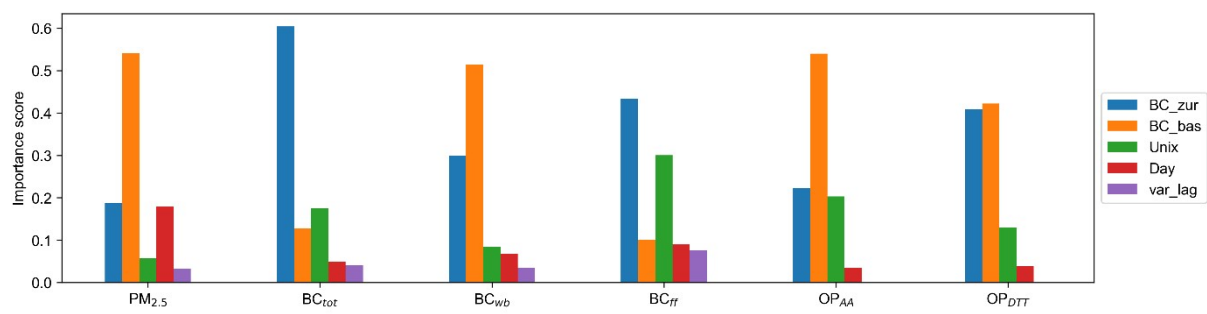

Figure S2: Feature importance score for the RF models performed on each target variable in the BERN (PM$_{2.5}$) site.
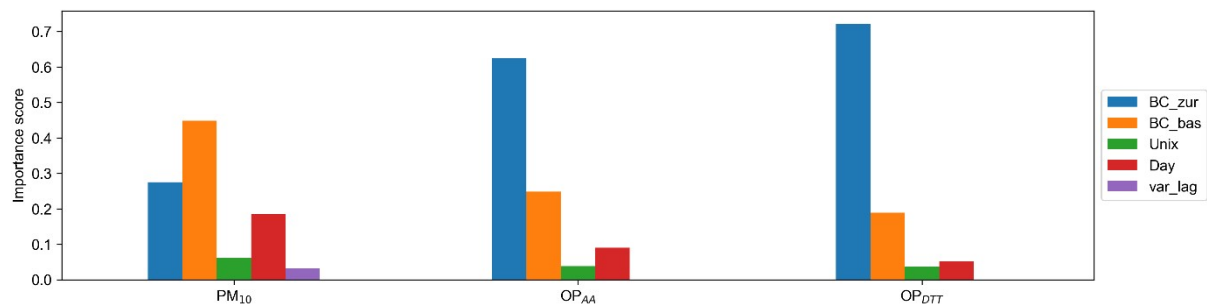

Figure S3: Feature importance score for the RF models performed on each target variable in the BERN (PM$_{10}$) site.

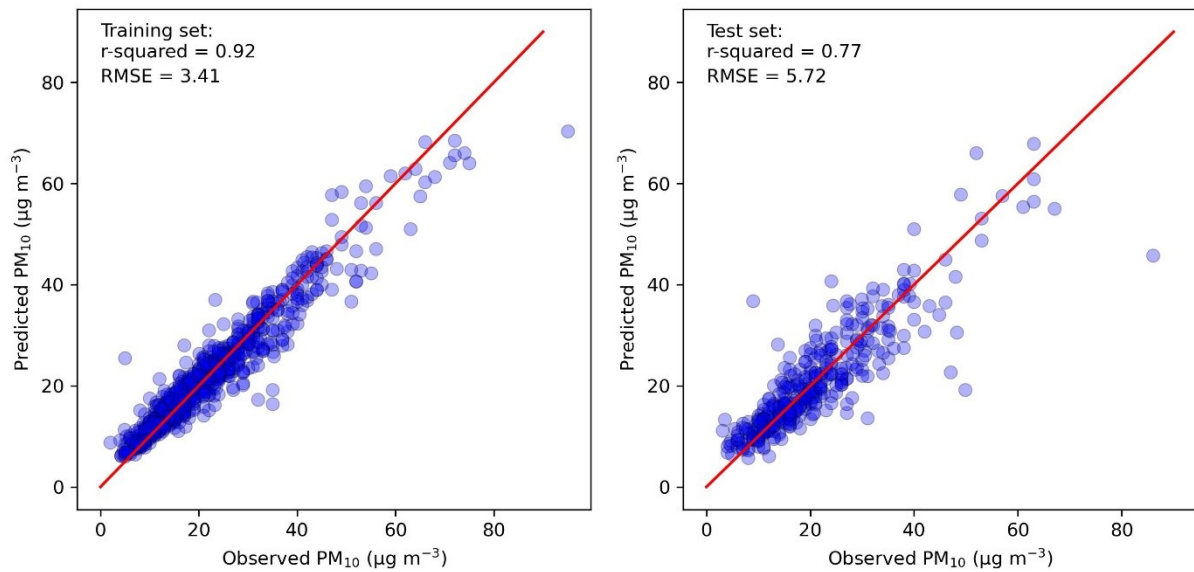## S3. Comparison of the Random Forest (RF) model performance between the training and testing sets

Figure S4: Comparison between the observed and RF- predicted PM$_{10}$ mass concentration (μg m^{-3}) for the training and testing sets in the GRE site. Note: Red line represents the one-to-one line.
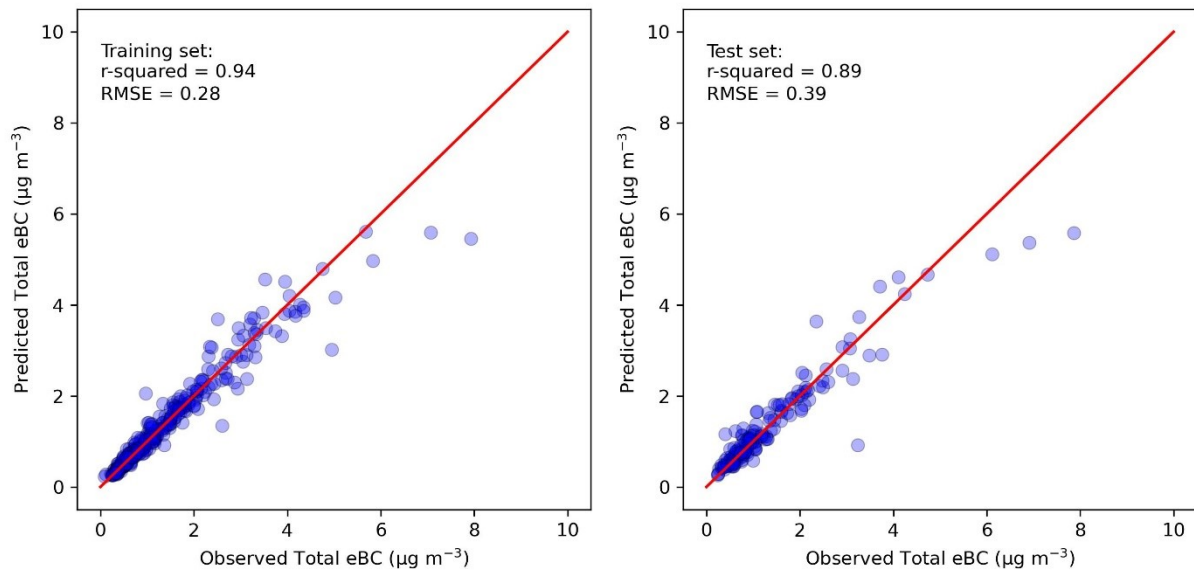

Figure S5: Comparison between the observed and RF- predicted total black carbon (BC$_{tot}$) mass concentration (μg m^{-3}) for the training and testing sets in the GRE site. Note: Red line represents the one-to-one line.
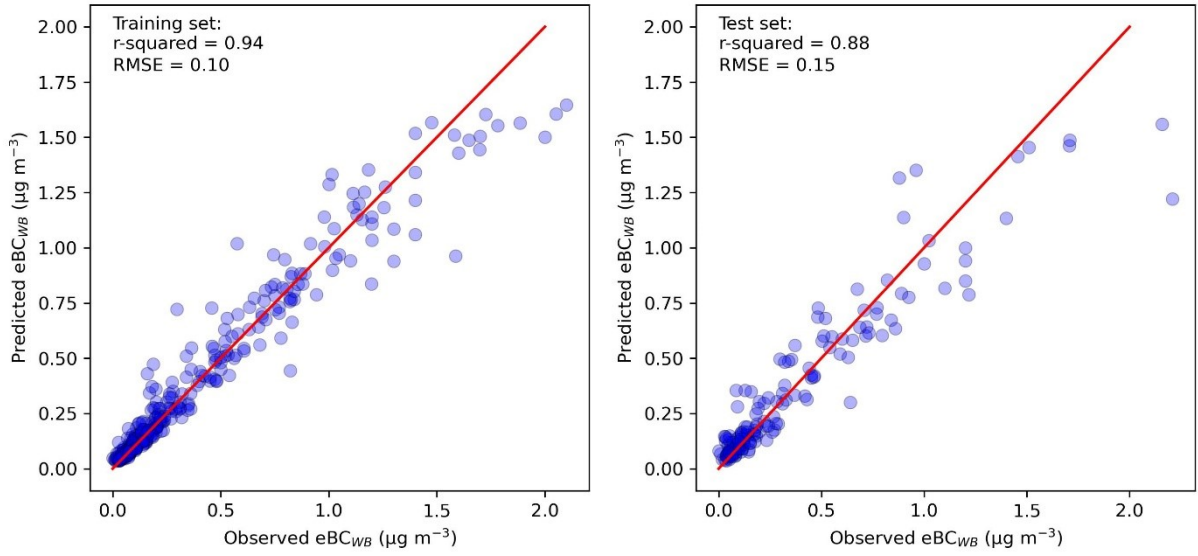
Figure S6: Comparison between the observed and RF- predicted wood burning black carbon (BC$_{wb}$) mass concentration (μg m^{-3}) for the training and testing sets in the GRE site. Note: Red line represents the one-to-one line.
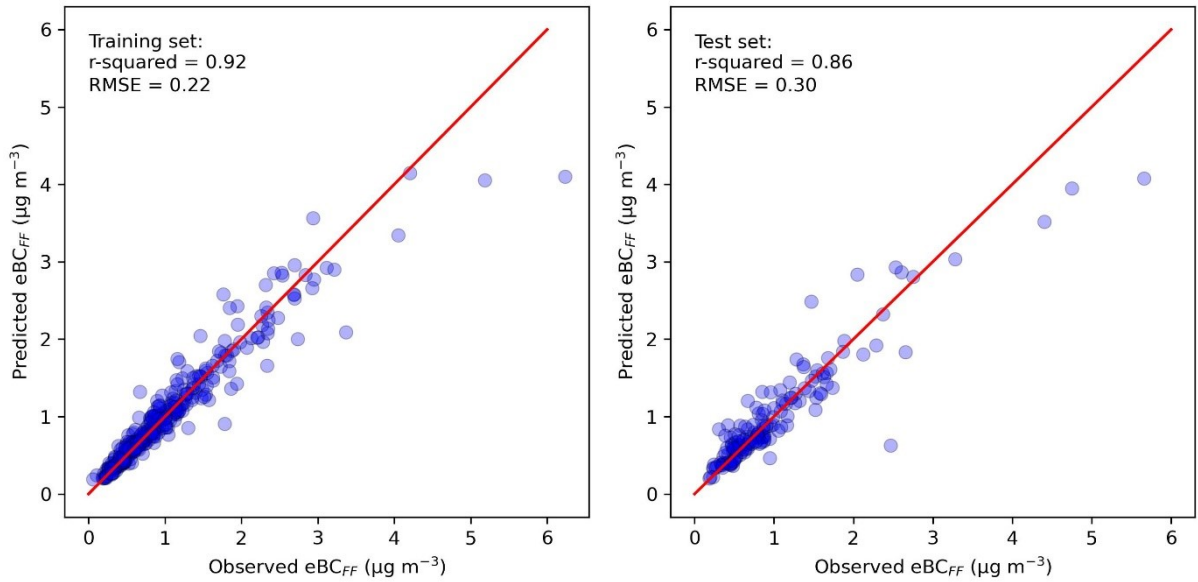

Figure S7: Comparison between the observed and RF- predicted fossil fuels black carbon (BC$_{ff}$) mass concentration (μg m^{-3}) for the training and testing sets in the GRE site. Note: Red line represents the one-to-one line.

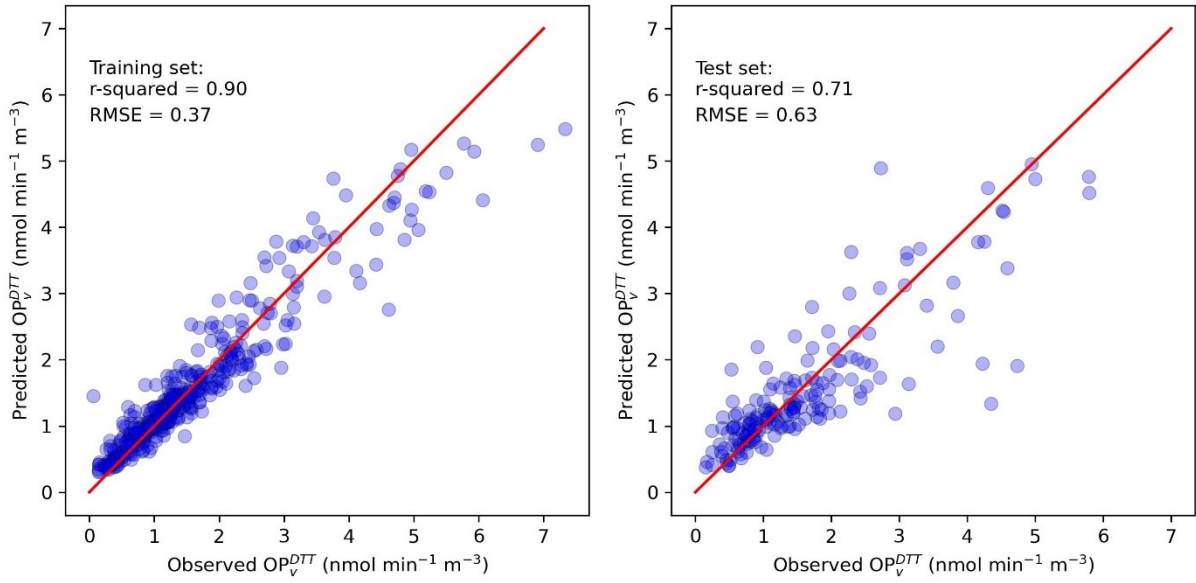**Figure S8: Comparison between the observed and RF- predicted OP$_{DTT}$ (nmol min^{-1} m^{-3}) of PM$_{10}$ for the training and testing sets in the GRE site. Note: Red line represents the one-to-one line.**
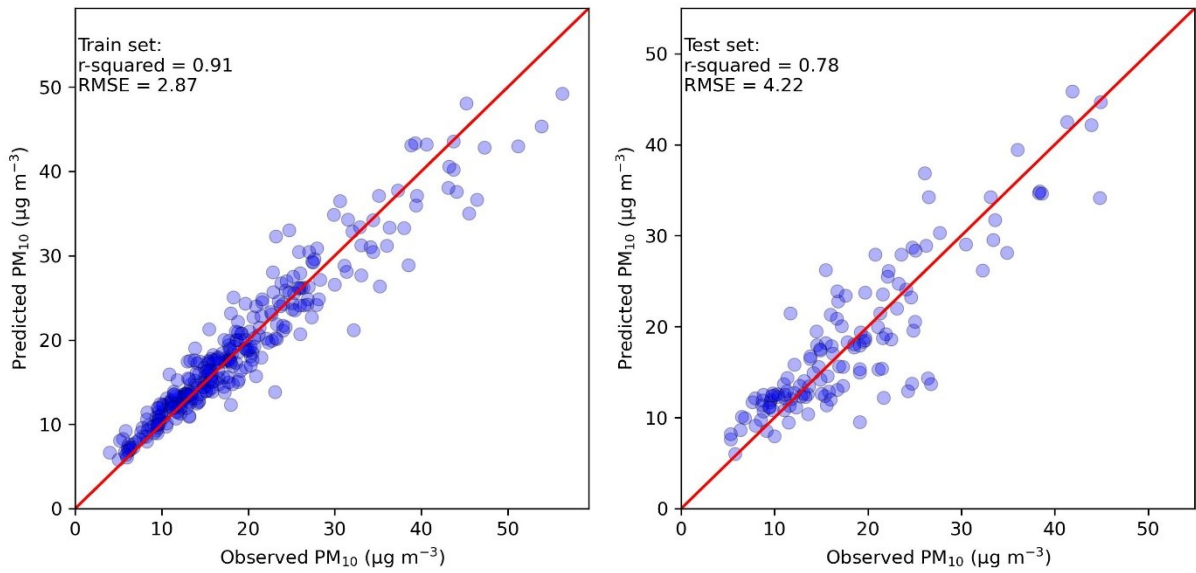

Figure S9: Comparison between the observed and RF- predicted PM$_{10}$ mass concentration (µg m^{-3}) for the training and testing sets in the BERN site. Note: Red line represents the one-to-one line.
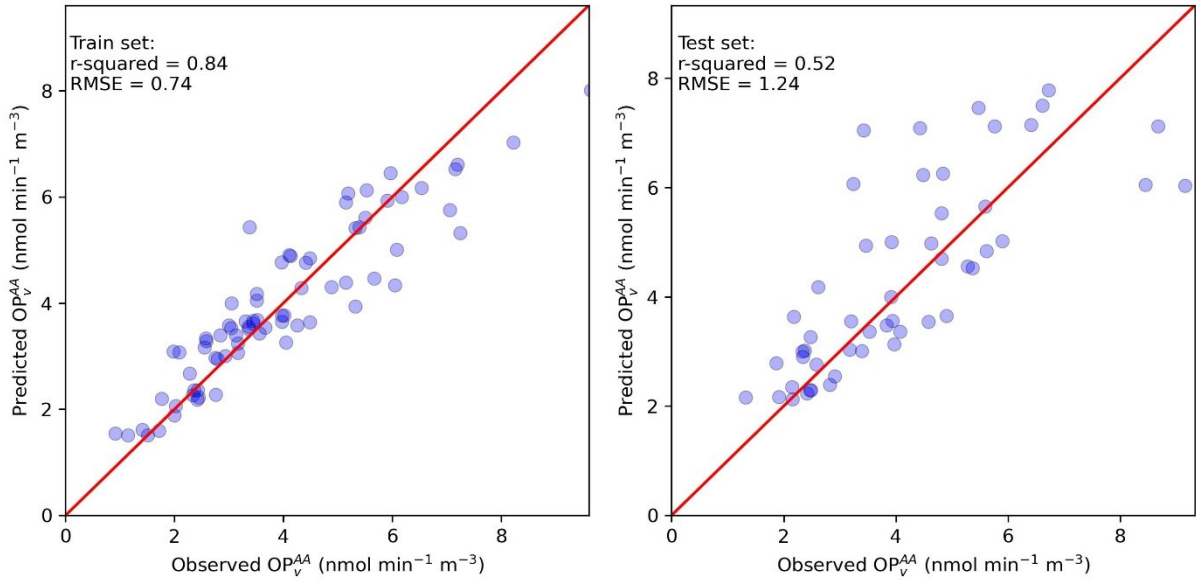
Figure S10: Comparison between the observed and RF- predicted OP_{AA} (nmol min^{-1} m^{-3}) of PM_{10} for the training and testing sets in the BERN site. Note: Red line represents the one-to-one line.
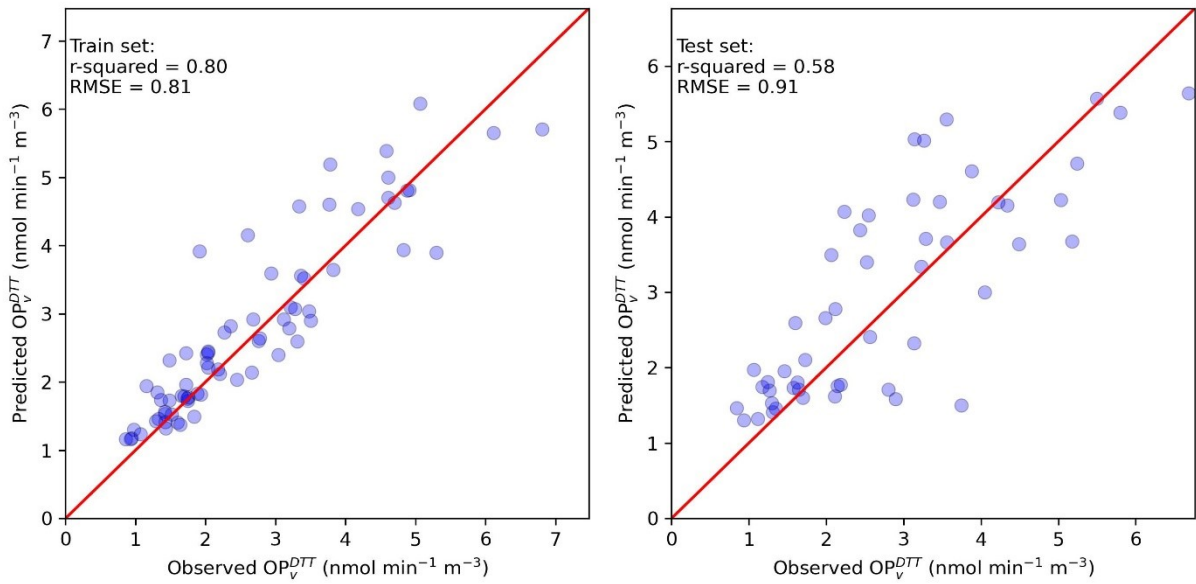
Figure S11: Comparison between the observed and RF- predicted OP_{DTT} (nmol min^{-1} m^{-3}) of PM_{10} for the training and testing sets in the BERN site. Note: Red line represents the one-to-one line.
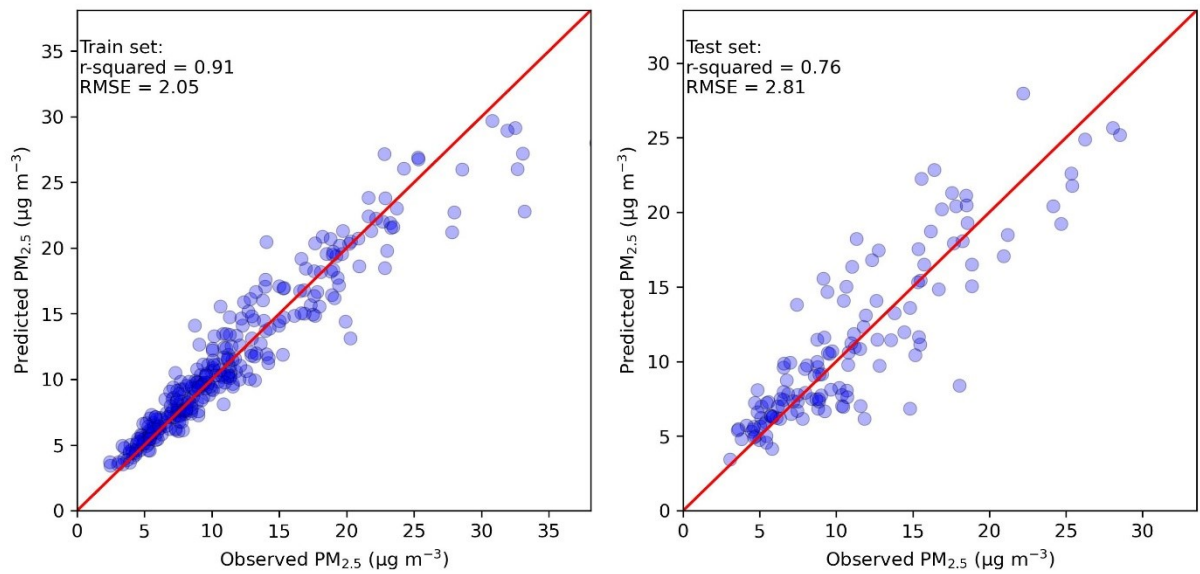
Figure S12: Comparison between the observed and RF- predicted PM$_{2.5}$ mass concentration (µg m^{-3}) for the training and testing sets in the BERN site. Note: Red line represents the one-to-one line.
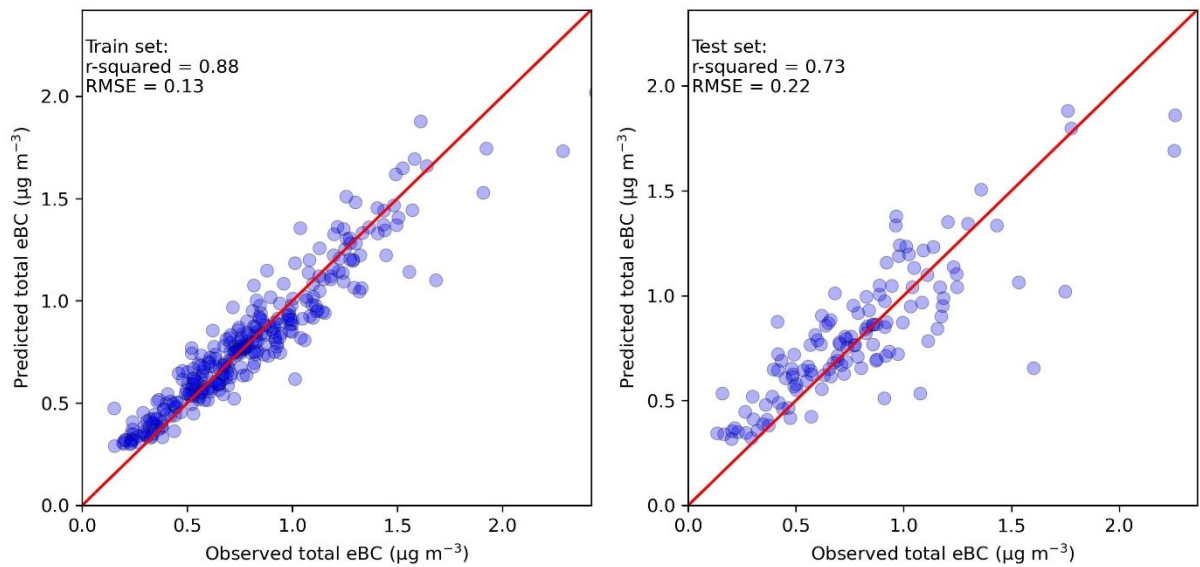

Figure S13: Comparison between the observed and RF- predicted total black carbon (BC$_{tot}$) mass concentration (µg m^{-3}) for the training and testing sets in the BERN site. Note: Red line represents the one-to-one line.
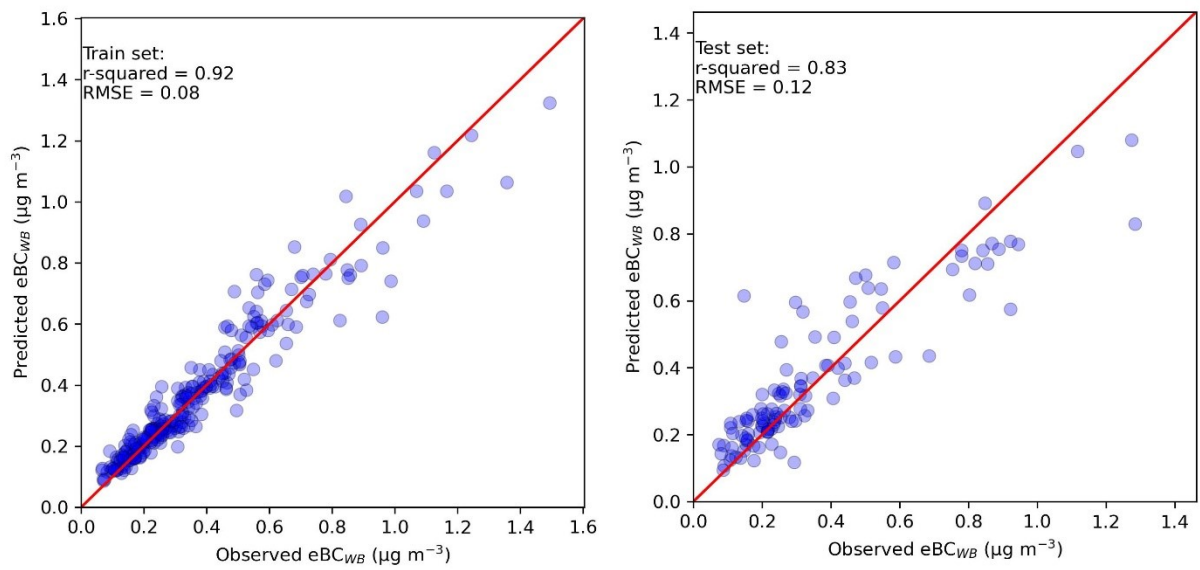
Figure S14: Comparison between the observed and RF- predicted wood burning black carbon (BC$_{wb}$) mass concentration (µg m^{-3}) for the training and testing sets in the BERN site. Note: Red line represents the one-to-one line.
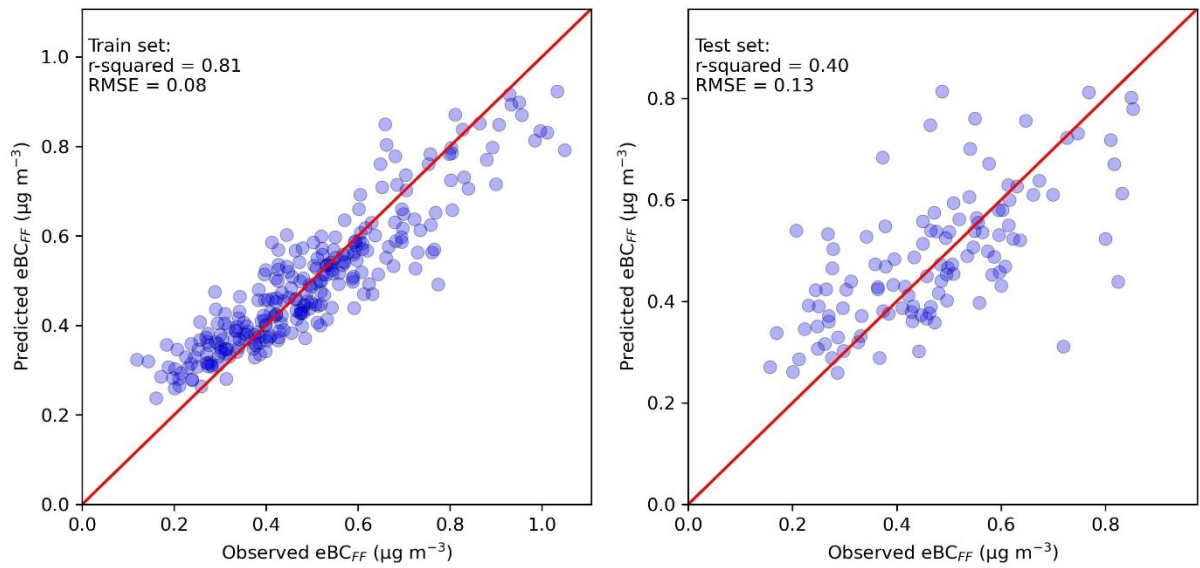

Figure S15: Comparison between the observed and RF- predicted fossil fuels black carbon (BC$_{ff}$) mass concentration (µg m^{-3}) for the training and testing sets in the BERN site. Note: Red line represents the one-to-one line.
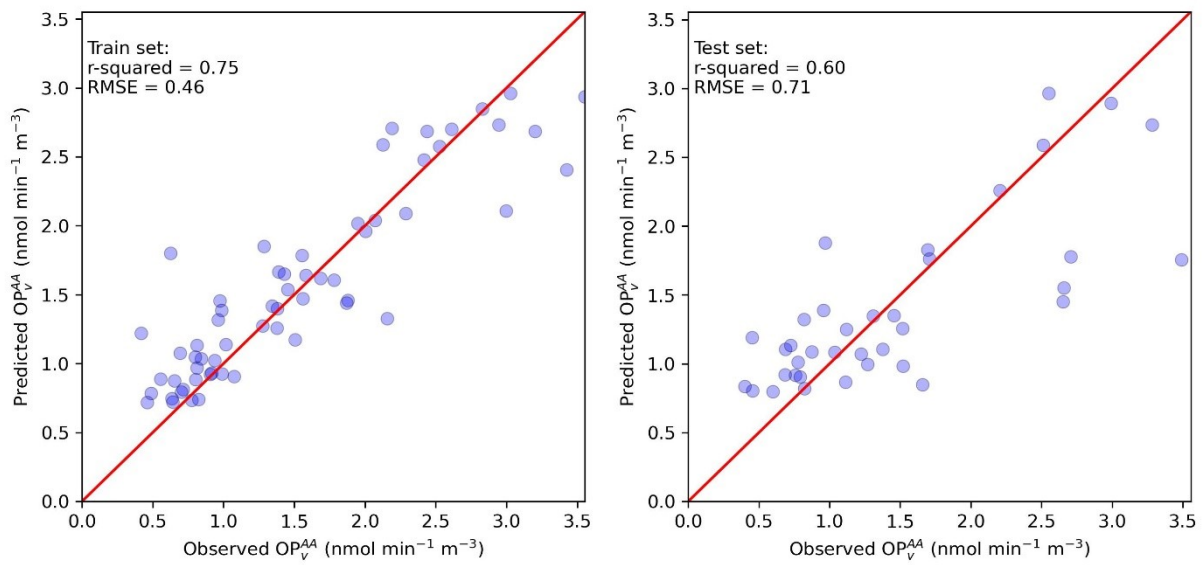
Figure S16: Comparison between the observed and RF- predicted OP_{AA} (nmol min^{-1} m^{-3}) of $PM_{2.5}$ for the training and testing sets in the BERN site. Note: Red line represents the one-to-one line.

Figure S17: Comparison between the observed and RF- predicted OP_{DTT} (nmol min^{-1} m^{-3}) of $PM_{2.5}$ for the training and testing sets in the BERN site. Note: Red line represents the one-to-one line.

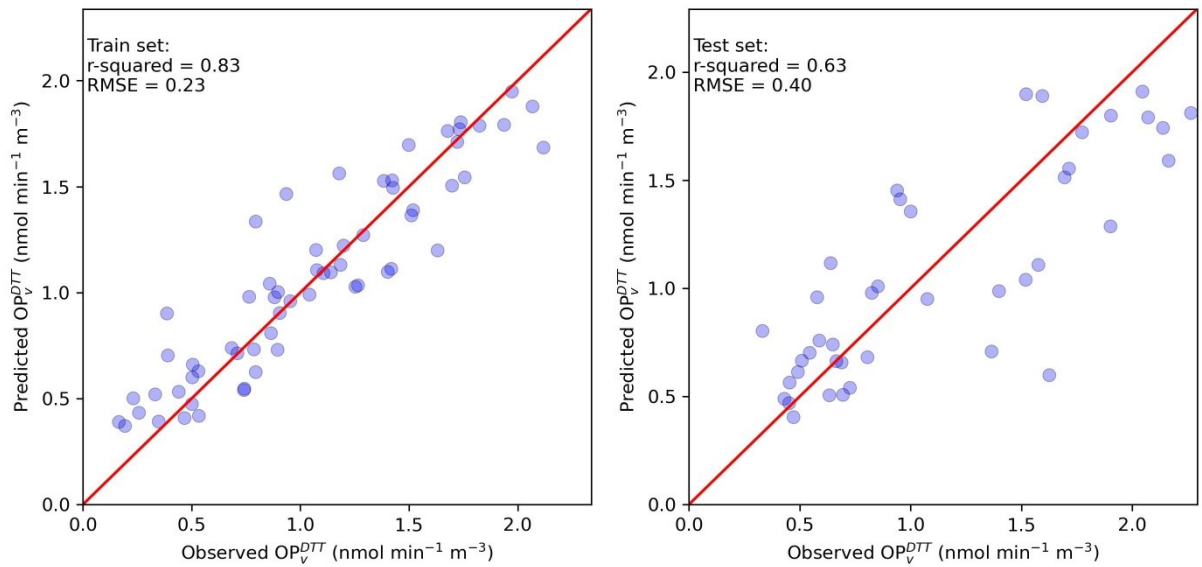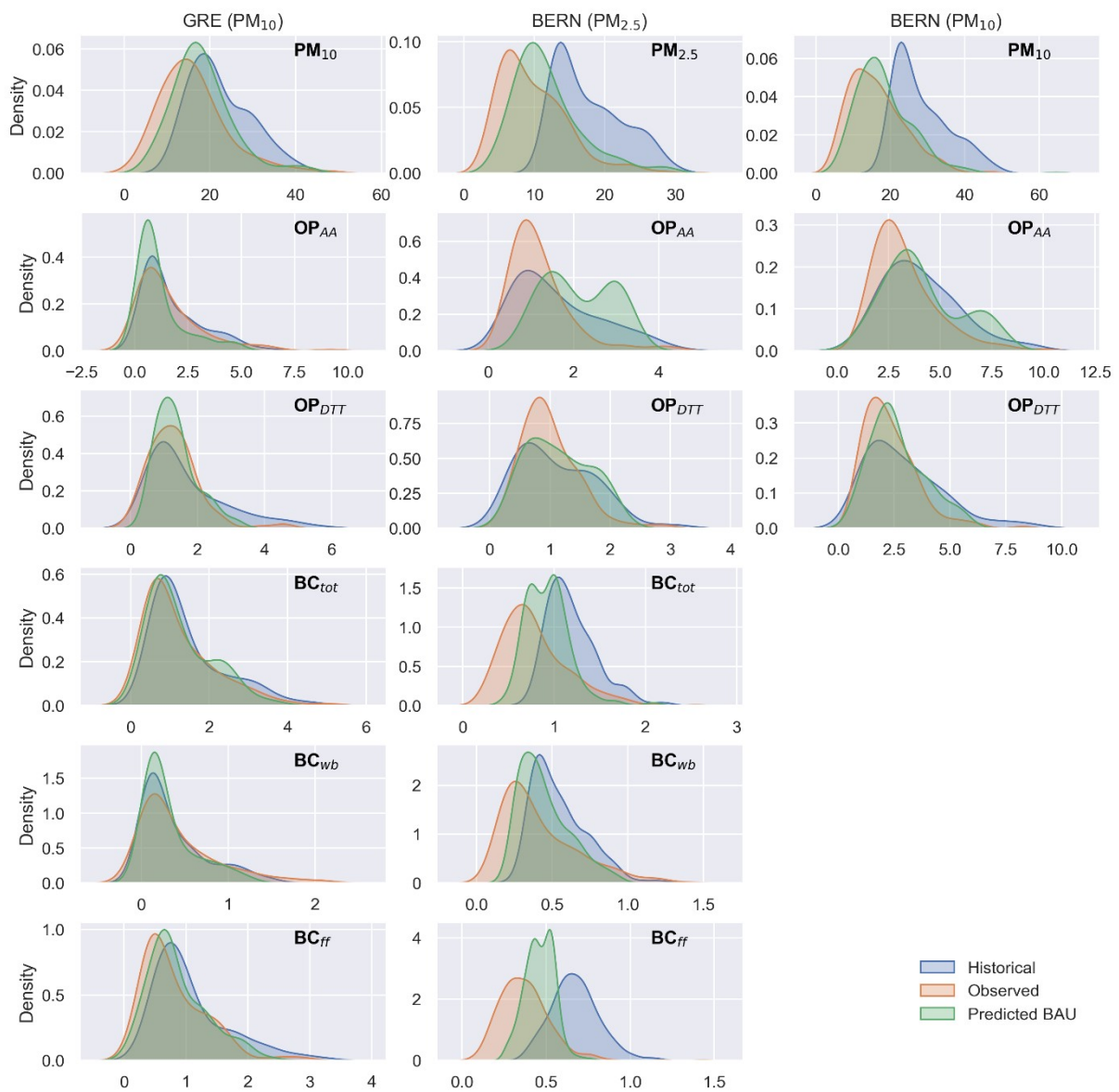## S3. Supplementary figures

Figure S18: Probability density plot between target variables (PM$_{10}$, BC$_{tot}$, BC$_{wb}$, BC$_{ff}$, OP$_{AA}$, and OP$_{DTT}$) in each site during the COVID-19 lockdown period. Blue curves represent historical levels prior to year 2020, the orange curves represent the observed levels during 2020, and green curves represent the RF-predicted business-as-usual (BAU) levels during 2020. Note: Each x-axis depicts the unit of each target variable: μg m^{-3} for PM$_{10}$, BC$_{tot}$, BC$_{wb}$, and BC$_{ff}$, while nmol min^{-1} m^{-3} for OP$_{AA}$ and OP$_{DTT}$.
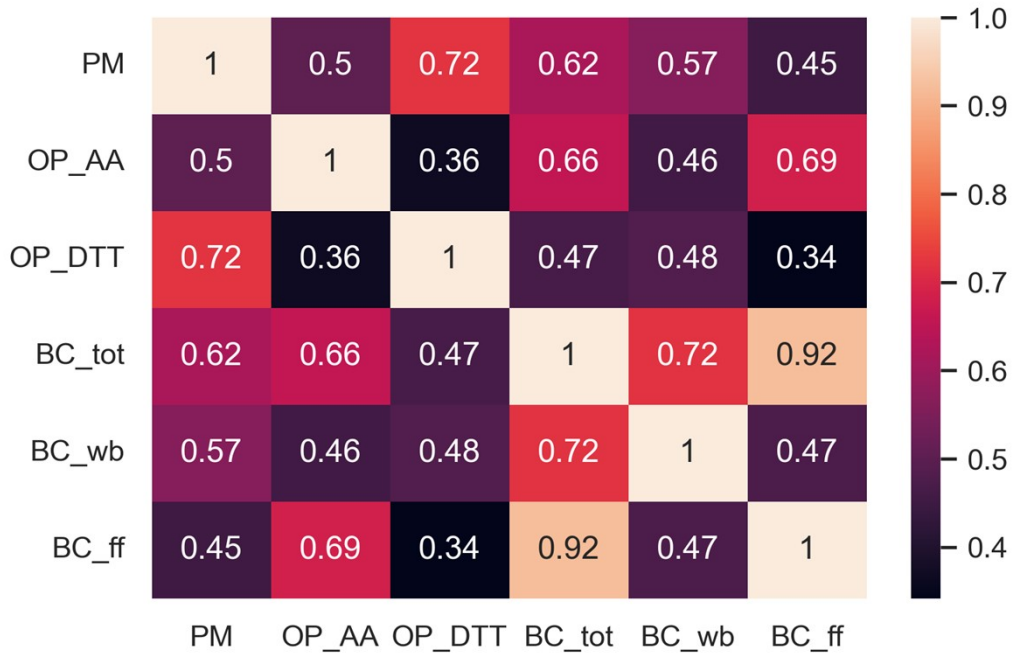
Figure S19: Heatmap of the associations of all variables in the PM$_{10}$ fraction using Pearson correlation in the GRE site.

Figure S20: Heatmap of the associations of all variables in the PM$_{10}$ fraction using Pearson correlation in the BERN site.
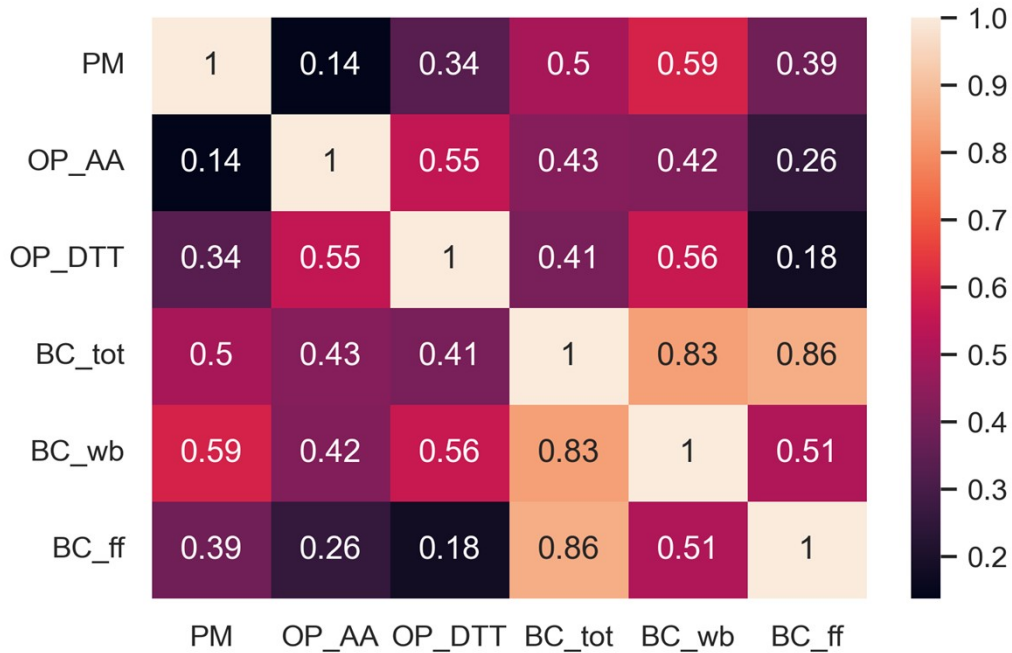
Figure S21: Heatmap of the associations of all variables in the PM$_{2.5}$ fraction using Pearson correlation in the BERN site.
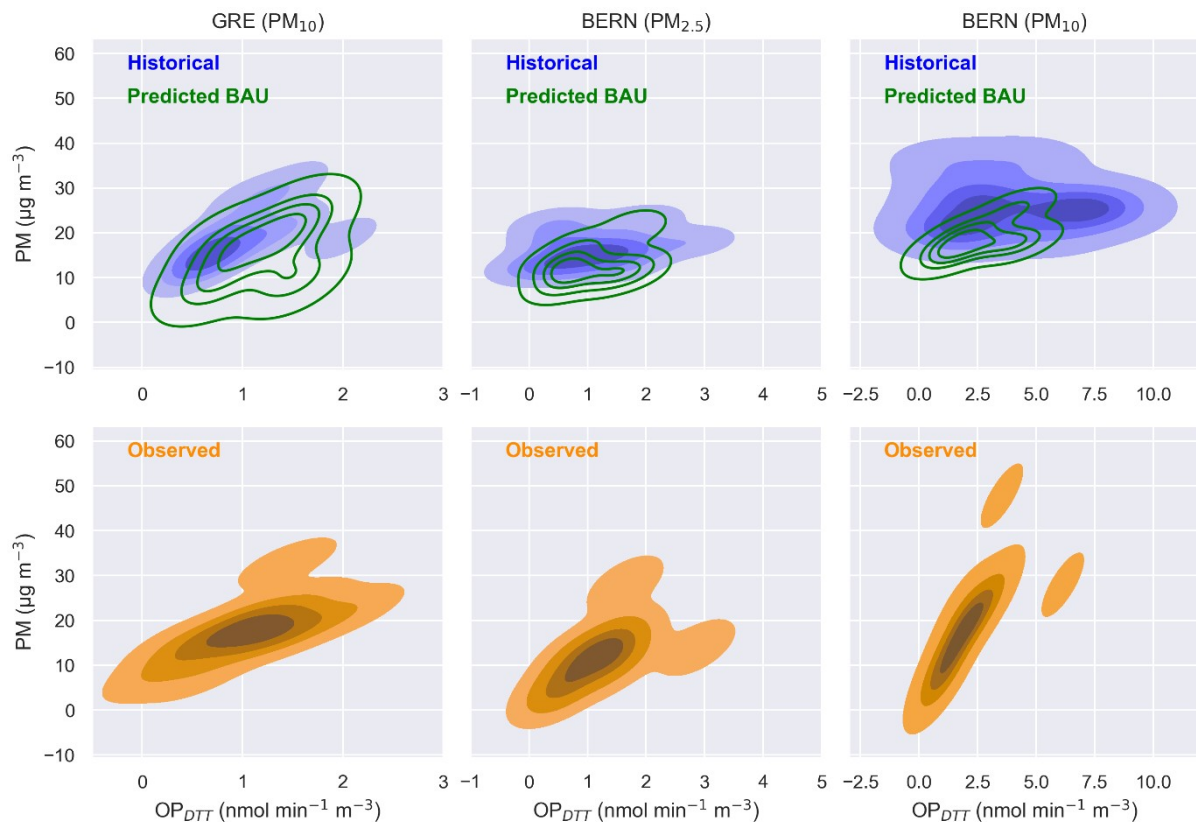

Figure S22: Bivariate distribution between PM and OP$_{AA}$ in each site during the COVID-19 lockdown period using a kernel density function (KDF). Blue plots represent historical levels prior to year 2020, the orange plots represent the observed levels during 2020, and green plots represent the RF-predicted business-as-usual (BAU) levels during 2020. Note: The default number of contours was set to 5 levels. These contours were drawn at *iso*-proportions of the density plot representing the distributions of both variables.